Growth of ZnO nanorods on FTO glass substrate

Growth of ZnO Nanorods on FTO Glass Substrate

Hamza Slimani[1], Noureddine Bessous[2], Sawsan Dagher[3*], Ali Hilal-Alnaqbi[4], Maisa El Gamal[5], Boshra Akhozheya[6], Mudasir Mohammed[3]

[1] *Department of Physics, University of El Oued, Fac. Exact Sciences, 39000 El Oued, Algeria*

[2] *Department of Electrical Engineering, University of El Oued, Fac. Technology, 39000 El Oued, Algeria*

[3]*Electromechanical Engineering Technology, Abu Dhabi Polytechnic, Abu Dhabi, UAE,*

[4]*Abu Dhabi Polytechnic, Abu Dhabi, UAE*

[5]*College of Natural and Health Sciences, Zayed University, Abu Dhabi, UAE*

[6]*Department of Building & Architectural Engineering, Polytechnic University of Milan, Milan, Italy*

* Corresponding author E-mail address: sawsan.dagher@adpoly.ac.ae

Abstract

A simple and direct method has been developed to grow zinc oxide (ZnO) nanorods (NRs) on a fluorine-doped tin oxide-coated glass (FTO) substrate. Firstly, spray pyrolysis deposition method is applied followed by dipping the substrate in a solution of ZnO growth reagents. The morphology, structure, and optical properties of the obtained thin film are investigated. The results demonstrate the successful synthesis of the ZnO NRs on FTO substrate. The NRs have a hexagonal rod like structure with diameter and length of 240 nm and 670 nm, respectively. FTO/ZnO NRs exhibited absorption of UV wavelengths and high transmittance in visible light region, with energy bandgap (E_g) of 3.2 eV. The characteristics of the FTO/ZnO NRs film can be explored in photovoltaic applications such as dye-sensitized solar cells.

Keywords: ZnO nanorods; Spray pyrolysis; FTO/ZnO; Thin films

Graphical Abstract

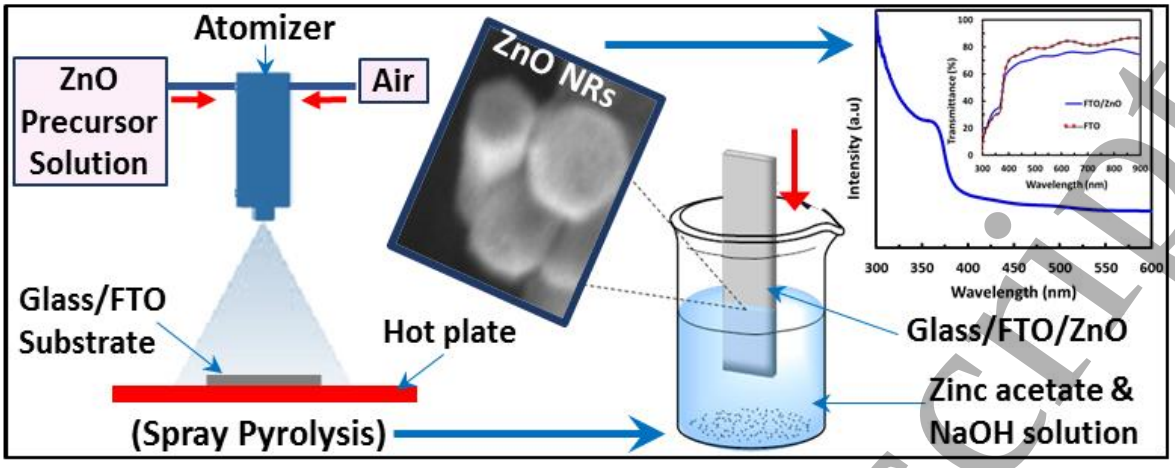

1. Introduction

Zinc oxide (ZnO) is a semiconductor with unique electrical and optical properties. This fact is due to its wide direct energy bandgap (E_g) of 3.37 eV, as well its large exciton binding energy (60 meV), and high electron affinity and mobility [1,2]. ZnO can be synthesized into diverse nanostructure configurations such as nanoparticles, nanowires, nanobelts, nanotubes and nanorods (NRs), in which its properties can be tailored to be utilized for wide range of specific applications. ZnO nanosized are used in photocatalysis [3], hydrogenation of carbon dioxide to methanol [4], gas and bio sensors [5,6], solar cells, and light-emitting diodes [7,8].

The size and shape, and consequently the properties of ZnO nanomaterial depends on the synthesis method, the precursor solution and the type of substrate [9, 10]. The most common methods to prepare ZnO NRs are; (i) Hydrothermal method: $Zn(NO_3)_2.6H_2O$ and Hexamethylenetetramine (HMTA) are used as precursors to grow ZnO NRs with diameter of 30 nm and length of 250 nm on a glass substrate [11], in another study zinc acetate ($Zn(CH_3COO)_2.2HO$), diaminopropane, and HMTA are used to synthesize ZnO NRs of 33 nm diameter and 1000 nm length on an alumina substrate [12]. Hydrothermal reactions occur at a relatively low temperature (200 °C) with long duration of synthesis (from about 10 hours to several days), moreover, the hydrothermal method is widely used to synthesize metal oxides nanostructures [13,14] (ii) Sonochemical method: $Zn(NO_3)_2.6H_2O$ and HMTA are used as precursors to grow ZnO NRs of 50 nm diameter and 500 nm length on an ITO coated glass substrate [15], in another study $Zn(CH_3COO)_2.2HO$ in paraffine oil is used to prepare ZnO NRs with diameter in the range of 40-80 nm and length in the range of 150-300 nm [16]. (iii) Electrochemical deposition: $ZnCl_2$ and KCl are used to synthesize ZnO NRs on porous silicon with diameter and length of 200 nm and 700 nm, respectively [17]. (iv) Spray pyrolysis: rods with diameter of 250 nm and length of 376 nm are synthesized on glass substrate using precursor solution of $ZnCl_2$ in distilled water [18]. (v) Chemical vapour deposition produces ZnO NRs with good crystallinity and high purity in a short time compared to other techniques, nevertheless, the vapour-phase reactions require a very high temperature (1400 °C) and require a complex vacuum system [19, 20]. Less common methods for ZnO NRs synthesis are pulsed laser deposition [21], RF magnetron sputtering [22], molecular beam epitaxy [23], and thermal evaporation [24]. However, these methods require specialized and complex equipment, or involve extremely high temperature, pressure or vacuumed system. Some examples on ZnO NRs' synthesis are shown in table 1 with few characteristics.

The synthesis of ZnO NRs on the fluorine-doped tin oxide-coated glass (FTO) substrate is essential for several photovoltaic and optoelectronic applications. However, there are few studies done on the growth of ZnO NRs on FTO substrate [25, 31], which is an effective transparent layer in solar cell structure that absorbs UV light and transfers electrons. In this study, we have proposed a simple, direct, and environment-friendly method to grow ZnO NRs on FTO substrate through two steps. This method offers several advantages such as the non-vacuum deposition, use of inexpensive equipment, relatively less complex and moderate temperatures are required for the growth of ZnO NRs compared to other deposition techniques. To the best of the authors' knowledge this is the first time to use $Zn(CH_3COO)_2.2H_2O$ and NaOH solution to synthesize ZnO NRs layer on FTO substrate, following a spray pyrolysis deposition step. As well, the morphological, structural and optical properties of the as synthesized FTO/ZnO NRs thin film are studied.

Table 1. Common synthesis methods of ZnO NRs, with their respective precursors, substrates, size range, and some other growth characteristics.

Preparation Method	**Precursors**	**Substrate**	**Diameter / Length (nm)**	**Ref.**	**Characteristics**
Hydrothermal	Zinc acitate, HMTA	Glass/ FTO	-	[25]	Reactions occur at a temperature of ~ 200 °C and high-pressure reaction conditions (eg. autoclave). Duration of synthesis is10 hours to several days.
Hydrothermal	$Zn(NO_3)_2.6H_2O$, HMTA	Alumina	100/1620	[26]	
Hydrothermal	$Zn(NO_3)_2{\cdot}6H_2O$, HMTA	Si wafer	200/3000	[27]	
Hydrothermal, calcination	Zinc acetylacetonat, urea		65/ 250	[28]	
Sonochemical	$Zn(NO_3)_2{\cdot}6H_2O$, HMTA	Glass/Ti	65.2 / 668.2	[29]	Ultrasound radiation is applied by means of acoustic cavitation. (high temperature and pressure is generated)
Electrochemical deposition	$Zn(NO_3)_2{\cdot}6H_2O$, K_2SO_4	Glass/ Indium Ti n Oxide (ITO)	diameters of 100-200	[30]	Temperature is <100 °C. Constant or pulsed current or potential can be applied. Ions from aqueous metal salt solutions (electrolyte) are deposited on the substrate (electrodes) to form ZnO.
Electrochemical deposition	$Zn(NO_3)_2{\cdot}6H_2O$, HMTA, KCl	Glass/ FTO	198-306 / 287-545	[31]	
Spray pyrolysis	zinc acetate solution	Glass	90 - 80 nm	[32]	Operating at temperatures of 100 - 500 °C. Involves atomization of precursor solution then evaporation and decomposition.
Spray pyrolysis	$Zn(NO_3)_2{\cdot}6H_2O$, HMTA	Glass	50-150/ 750-780	[33]	

2. Experimental methods

ZnO NRs were deposited on fluorine-doped tin oxide (SnO_2/F) glass substrate. Initially the FTO substrate was cleaned by successive sonication in acetone and methanol, then the substrate was rinsed with deionized water (H_2O) and dried with nitrogen gas (N_2).

In the first step; The precursor material zinc acetate dehydrated (Zn $(CH_3COO)_2 \cdot 2H_2O$) was dissolved in H_2O/methanol (1/2). With a concentration of 0.3 M. and 2 drops of glacial acetic acid (CH_3COOH) was added to avoid flakes formation. The solution was deposited on the FTO substrate using spray pyrolysis method to initiate the ZnO seed layer. The substrate temperature was fixed at 450 °C and the substrate to nozzle distance was 5 cm, then the substrate was sprayed on using a solution which was atomized by compressed ambient air at the pressure of 2 bar. The solution's flow rate was kept at 1ml/min and the number of deposition sequences was 7. Then the substrate was left to cool at room temperature.

In the second step, 1.81 mmol of each of the $Zn(CH_3COO)_2.2H_2O$ and NaOH were dissolved in 100 mL of ethanol under rigorous magnetic stirring. The substrate was dipped in the solution for 1 hour at constant temperature of 65 °C which simulates the growth of NRs. Finally the substrate was washed in H_2O and dried with N_2. The chemical reaction for ZnO NRs growth can be described as follows [34]:

$$5Zn(CH_3COO)_2{:}2H_2O \longrightarrow Zn_5(OH)_8(CH_3COO)_2 + 2CH_3COOH$$

$$Zn_5(OH)_8\,(CH_3COO)_2 + 2NaOH \longrightarrow 5ZnO + 2NaCH_3COO + 5H_2O$$

The formation mechanism of the ZnO NRs can be explained as follows; during spray pyrolysis process, when precursor solution droplets arrive close to the FTO substrate which is heated at 450°C, the droplets undergo thermal decomposition, leading to the formation of the highly adherent (to the substrate) seed layer of ZnO nanocrystals. The ZnO seed layer surface has a high reactivity because of the energy supplied via the heat treatment at 450°C during the synthesis process. Therefore, in the second stage; as the substrate dipped into the solution of precursors the Zn^{2+} and OH^- ions (present in the solution) are diffused in the ZnO seeds, resulting in the increase of their length and diameter to develop the ZnO NRs structure. Thus, in this process, the ZnO nanocrystals in the seed layer served as nucleation centers for the subsequent growth of ZnO NRs.

The morphology and crystallographic structure of synthesized FTO/ZnO NRs was characterized using scanning electron microscope (SEM) with an energy dispersive X-ray spectroscopy (EDS) facility (JSM-5600; JEOL, Japan), Fourier transform infrared spectroscopy (FTIR, Nexus TM 670), and powder X-ray diffractometer (XRD, Shimadzu, 6100, Japan) using Cu Kα radiation (λ = 1.5405 A°). The absorption and transmission spectra were measured using UV-Vis-NIR spectrophotometer (Perkin Elmer LAMBDA 950).

3. Results and discussion

3.1. Morphology and structure of the FTO/ ZnO NRs

Figure 1 displays the SEM images of the ZnO layer deposited on FTO glass substrates. Figure 1(a) shows a side view of the FTO/ZnO film, results indicate that ZnO is will coated on FTO surface with thickness of 680 nm. Figure 1(b-d) show the formation of rod-like nanostructure with a hexagonal columnar structure. The approximate diameter and length of the rods is 240 nm and 670 nm, respectively. The ZnO NRs have grown in multiple directions to the substrate.

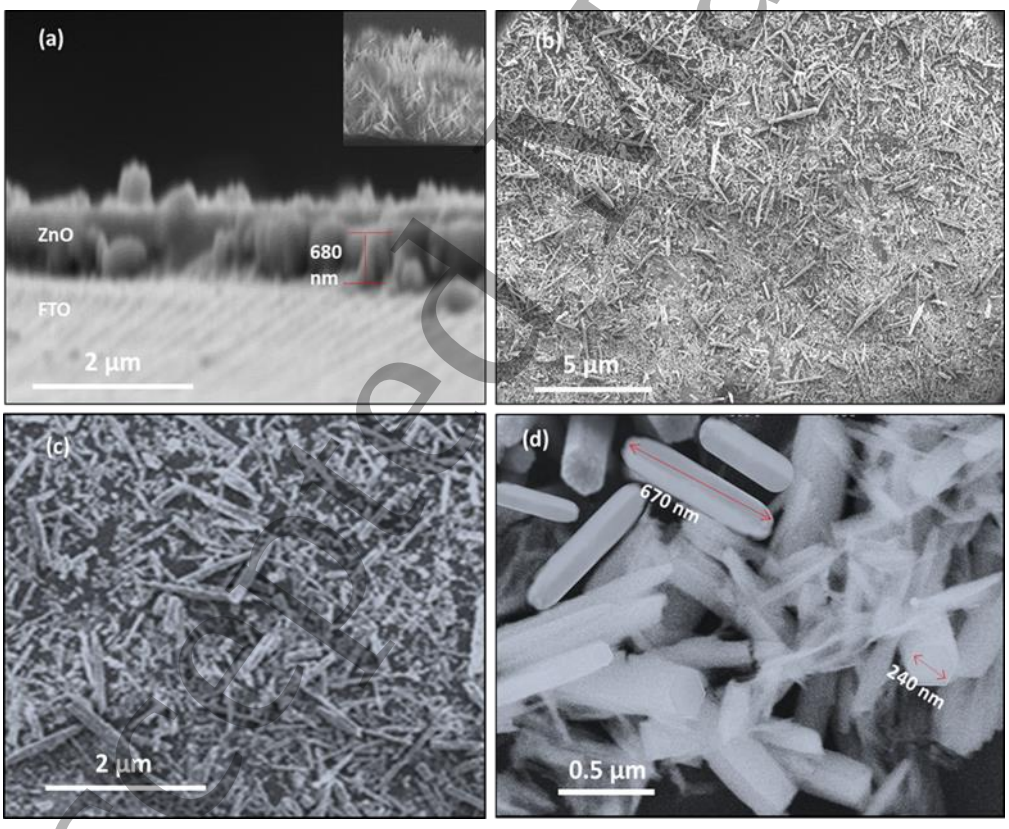

Figure 1. SEM images Of FTO/ZnO nanorods.

Figure 2 (a) shows XRD patterns as 2θ in the range of 10°-70° for the FTO/ZnO NRs. The 2θ values of 31.61°, 34.33°, 36.10°, 47.36°, 56.31°, 62.64°, 67.64°, and 68.73° are related to the crystal planes (100), (002), (101), (102), (110), (103), (112) and (201), respectively. The assigned diffraction peaks specify the hexagonal crystal structure of ZnO with cell parameters of a = 3.249 Å and c = 5.206 Å (JCPDS card no. 79-0208). It indicates a high orientation in the c-axis. The diffraction peaks at 2θ of 26.5, 37.9, 51.6, and 54.6 are assigned to tin oxide (SnO_2) from FTO substrate (JCPDS card no. 41-1445). Very few additional weak peaks appeared (with insignificant intensity), which could be attributed to the remaining organic components such as: $C_4H_6O_4Zn_2H_2O$, $C_2O_4Zn_2H_2O$, $Zn(OH)_2$ or zinc acetate, and this is anticipated in wet-chemical reactions due to the salts and solvents used.

Figure 2 (b) shows FTIR spectrum of FTO/ZnO in the range of 4000-400 cm^{-1}. The broad band at 3433 cm^{-1} is corresponding to the O-H stretching mode of the hydroxyl group. The hydroxyl groups are found on the surface because of the hygroscopic nature (i.e., adsorption of water molecules from the surrounding environment) of the ZnO NRs, the substrate was also washed with H_2O in the final stage of ZnO NRs growth. The observed peaks at 1703, 1624, 1124, 927, and 700 cm^{-1} are attributed to the symmetric and asymmetric stretching of the zinc hydroxyl group. The weak peak at 1415 cm^{-1} might be assigned to the symmetric stretching of carboxylate group (COO-), and the weak peaks at 1550 cm^{-1} and 1665 cm^{-1}, are due to asymmetric C=O bonds vibrations, possibly originated from reaction intermediates such as a minor residue of zinc acetate used in the reaction. The peak at 482 cm^{-1} is assigned to the stretching vibrations of ZnO. The peak at 735 cm^{-1} is due to the Zn-O bonding, are clearly represented [35]. Collectively, these observations confirm the formation of the ZnO layer.

The spectra in the bottom inset shows the elemental two-dimensional energy-dispersive spectroscopy analysis for FTO/ZnO surface. The mass percentage of these elements are shown in the table (above inset). Sn and F elements can be seen, in addition to Zn and O elements, which indicates the migration of these elements to the surface and could be a result of uncoated areas. Also, XRD patterns indicated few diffraction peeks resulted from FTO.

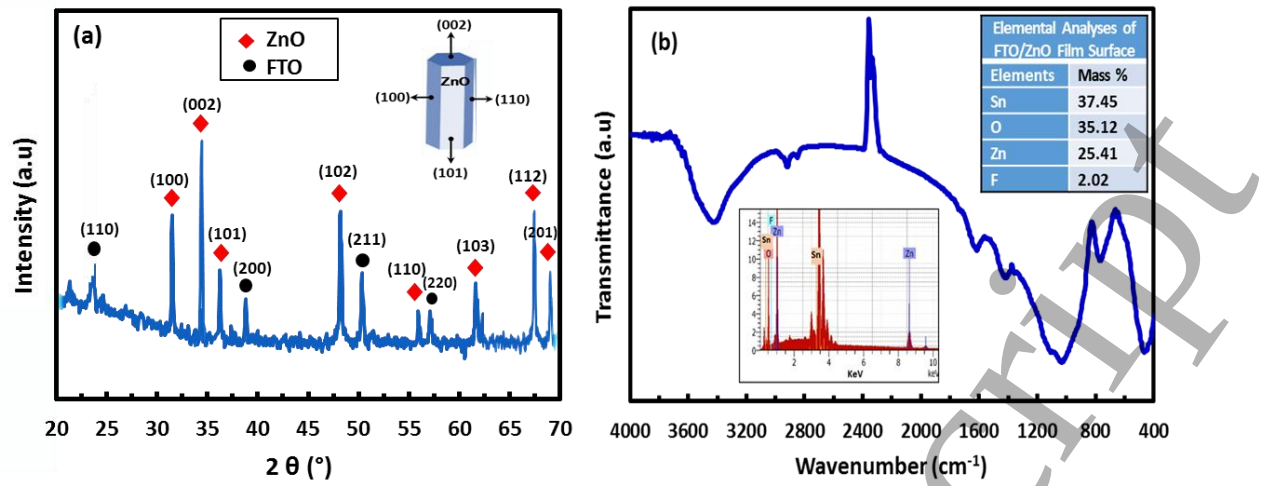

Figure 2. (a) XRD patterns of FTO/ZnO film, (b) FTIR spectra of FTO/ZnO NRs, and the insets are their energy-dispersive X-ray spectroscopy elemental analysis.

3.2 Optical properties

Figure 3 (a) shows UV- UV-Vis light absorption spectrum of the prepared FTO/ZnO NRs. It is clear that the film exhibits absorption in the UV light region. The spectrum can be used to estimate the optical energy band gap (Eg) in eV based on the Tauc's formula [36]:

$$(\alpha h\nu)^n = B(h\nu - E_g)$$

Where α is the absorption coefficient (cm^{-1}), hν is the photon energy (eV), B and n are constants, n is 2 for direct electronic transition. The E_g can be calculated by creating a graph of $(\alpha h\nu)^2$ versus hν, thus the E_g value is the intersection of the extended straight line of the linear portion of the curve to the X axis, as shown in the inset in figures 3(a). The linearity of the curve indicates that the ZnO NRs have direct band gap transitions. The estimated E_g for FTO/ ZnO NRs is 3.2 eV. The E_g values of these NRs are less than the E_g of their bulk (3.37), even though usually as crystal size decreases the E_g increases because of the quantum confinement effects [1, 34]. However, the results in this study show a decrease in the E_g value in comparison to the bulk. This can be attributed to the effect of FTO substrate, which indicates that few oxygen (O) atoms are replaced by Fluorine (F) atoms in ZnO. EDS analysis for FTO/ZnO surface (shown in the inset of Figure 2b) indicate the presence of F element on the film surface, with a mass percentage of 2.02 %. The integration mechanism of F into the surface, can occur via three main routes; (i) F bonds to OH groups onto the surface by the formation of intermolecular hydrogen bonds (OH-F), (ii) F atoms occupy the oxygen vacancies, (iii) Some O atoms might be substituted by F atoms into oxygen lattice sites because their ionic radii are the same. Thus, the small reduction in E_g might be due to the creation of energy levels in the band gap near the conduction band.

Figure 3 (b) shows the transmittance spectra of Pure FTO and FTO/ ZnO NRs thin films. The films demonstrated extraordinary transmittance values in the visible range (380-780nm), while remarkable decrease in transmission in the UV domain is observed. Pure FTO and FTO/ZnO film showed transmission of 87% and 78%, respectively, in the visible wavelength light. The high optical transparency of the FTO/ZnO film confirms the high crystallinity of the as synthesized ZnO NRs [37].

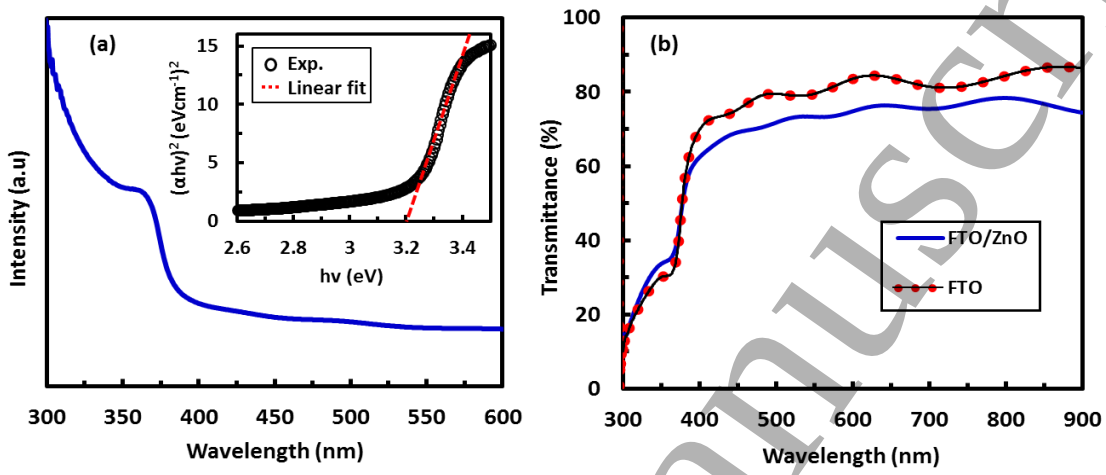

Figure 3. (a) UV–visible absorption spectrum of FTO/ ZnO thin film, the inset is its Tauc plot, (b) Transmittance spectra of FTO/ ZnO thin film.

In summary, the synthesized ZnO NRs showed hexagonal wurtzite structure which is more stable than zinc blende structure at ambient temperatures. It is known that the ZnO has a strong ionic bond with the radii of Zn^{2+} being 0.074 nm and for O^{2-} being 0.140 nm. This property further enhances the formation of hexagonal wurtzite structure, and the tendency of crystallization along c-axis, thus, a rod-liked structure is obtained. The synthesized ZnO NRs exhibited a lattice constants ratio c/a of 1.60, mostly similar to that of the hexagonal cell's ideal value (c/a=1.633). Thus, the high crystallinity degree of the ZnO NRs is indicated by the high intensity of the XRD peaks [38].

The optical analysis also verified the structural characteristics. Due to the fact that the transmittance increases with increasing crystalline quality, FTO/ZnO film demonstrated an excellent transmittance in visible and IR wavelength. In addition, the red shift in the E_g value indicates the enhanced crystallinity of the thin film [39]. Several researches have been done to decrease the E_g of ZnO by doping with other metals such as Fe, Cu, Al Ag. However, in this method the obtained FTO/ ZnO NRs demonstrates optical band gap of 3.2 eV value. This decrease in E_g value could be related to changes in the electronic structure of ZnO such as the

presence of closely sited acceptor levels in the region between the valence and conduction bands (i.e., forbidden bandgap).

Conclusions

Successful growth of ZnO NRs on FTO substrate was achieved via a simple yet efficient method; firstly, ZnO seed layer is initiated by spray pyrolysis method, then the complete growth of ZnO NRs is achieved by using $Zn(CH_3COO)_2.2H_2O$ and NaOH solution at relatively low temperature. The obtained film is investigated by various characterization techniques. SEM images and XRD patterns confirm the formation of hexagonal crystal structure ZnO NRs, with diameter of 240 and length of 670 nm. The E_g of ZnO NRs exhibits a slight red-shift compared to their bulk, due to the effect of FTO substrate layer. Moreover, FTO/ZnO NRs thin film shows high visible light transmittance. The produced FTO/ZnO could be used as an effective electron transport layer and UV detector for photonic, optoelectronic and photovoltaic applications.

References

1. N. Tit, S. Dagher, A.I. Ayesh, Y. Haik, Adv. Sci. Eng. Med. 6 (2014) 1158.
2. N. Tit, S. Dagher, A.I. Ayesh, Y. Haik, J. Electron. Mater. 41 (2012) 3111.
3. A. Udoma, M.K. Ram, E.K. Stefanakos, A.F. Hepp, D.Y. Goswami, Mat. Sci. Semicond. Proc. 16 (2013) 2070.
4. M. Mureddu, F. Ferrara, A. Pettinau, Appl. Catal. B-Environ. 258 (2019) 117941.
5. N. Nasiri, Ch. Clarke, Biosensors *9* (2019) 43
6. Ganesh Kumar Mani, John Bosco Balaguru Rayappan, Mater. Lett. 158 (2015) 373.
7. A. Saboor, S. M. Shah, H. Hussain, Mat. Sci. Semicond. Proc. 93 (2019) 215.
8. S. Dagher, Y. Haik, N. Tit, A.I. Ayesh, J. Mater. Sci. Mater. El. 27 (2015) 3328.
9. G.Ch. Yi, Ch. Wang, W. Park, Semicond. Sci. Technol. 20 (2005) 22.
10. S. M. Karadeniz, M. Ö. Yeşilyurt, Surfaces and Interfaces 18 (2020) 100418.
11. S. Ozturk, N. Kılınc¸, Z.Z. Ozturk, J. Alloys Compd. 581 (2013) 196.
12. F.T. Liu, S.F. Gao, S.K. Pei, S.C. Tseng, C.H.J. Liu, J. Taiwan Inst. Chem. E. 40 (2009) 528.
13. W. Zhong, J. Huang, S. Liang, J. Liu, Y. Li, G. Cai, Y. Jiang, J. Liu, ACS Energy Lett., 5 (2020) 31-38.
14. Y. Mo, Z. Tan, L. Sun, Y. Lu, X. Liu, J. Alloys Compd. 812 (2020) 152166.

15. E. Oh, H.Y. Choi, S.H. Jung, S. Cho, J.C. Kim, K.H. Lee, S.W. Kang, J. Kim, J.Y. Yun, S.H. Jeong, Sensor Actuat. B-Chem. 141 (2009) 239.
16. X. Zhang, H. Zhao, X. Tao, Y. Zhao, Z. Zhang, Mat. Lett. 59 (2005) 1745.
17. D. Yan, M. Hu, S. Li, J. Liang, Y. Wu, S. Ma, Electrochim. Acta 115 (2014) 297.
18. S.J. Ikhmayies, M.B. Zbib, J. Electron. Mater. 46 (2017) 3982.
19. C. Rodwihok, S. Choopun, P. Ruankham, A. Gardchareon, S. Phadungdhitidhada, D. Wongratanaphisan, Appl. Surf. Sci. 477 (2019) 159-165.
20. E. Danielson, V. Dhamodharan, A. Porkovich, P. Kumar, N. Jian, Z. Ziadi, P. Grammatikopoulos, V. A. Sontakke, Y. Yokobayashi & M. Sowwan, Sci. Rep. 9 (2019) 17370.
21. C.F. Lin, M.S. Lin, C.C. Chen, P.H. Tsai, F.H. Wang, Surf. Coating. Technol. 231 (9) (2013) 161.
22. S.W. Kang, S.K. Mohanta , Y.Y. Kim, H.K. Cho, Cryst. Growth Des. 8 (2008) 1458.
23. Y.W. Heo, V. Varadarajan, M. Kaufman, K. Kim, D.P. Norton, Appl. Phys. Lett. 81 (2002) 3046.
24. A. Umar, Y.B. Hahn, Appl. Phys. Lett. 88 (2006) 173120
25. K.A. Adegoke, M. Iqbal, H. Louis, O.S. Bello, Mat. Sci. Energy Tech. 2 (2019) 329.
26. Y. Sahin, S. Ozturk, N. Kılınc, A. Kosemen, M. Erkovane, Z.Z. Ozturk, Appl. Surf. Sci. 303 (2014) 90.
27. P. Dash, A. Manna, N. C. Mishra, Shikha Varma, Physica E: Low-dimensional Systems and Nanostructures 107 (2019) 38.
28. R. Gao, X. Cheng, Sh. Gao, X. Zhang, Y. Xu, H. Zhao, L. Huo, Appl. Surf. Sci. 485 (2019) 266.
29. N.A. Hammed, A.A. Aziz, A.I. Usman, M.A. Qaeed, Ultrason. Sonochem., 50 (2019) 172.
30. C. Yilmaz, U. Unal, Appl. Surf. Sci. 368 (2016) 456.
31. T. Marimuthu, N. Anandhan, R. Thangamuthu, Appl. Surf. Sci. 428 (2018) 385.
32. S.D. Shinde, G.E. Patil, D.D. Kajale, V.B. Gaikwad, G.H. Jain, J. Alloys Compd. 528 (2012) 109.
33. E. Karaköse, H. Çolak, Energy 140 (2017) 92.
34. S. Dagher, A.I Ayesh, N. Tit, Y. Haik, Mat. Technol. Adv. Perf. Mat. 29 (2014) 76.
35. T. Ivanova, A. Harizanova, T. Koutzarova, B. Vertruyen, Mat. Lett. 64 (2010) 1147.
36. S. Dagher, Y. Haik, A.I. Ayesh, N. Tit, J. Lumin. 151 (2014) 149.
37. Z.C. Chen, L.J. Zhuge, X.M. Wu, Y.D. Meng, Thin Solid Films 515 (2007) 5462.
38. J. Qi, J. Chang, X. Han, R. Zhong, M. Jiang, Z. Chen, B. Liu, Mater. Chem. Phys. 211 (2018) 168.
39. S. Ilican, Anadolu University Journal of Science and Technology. A: Applied Sciences and Engineering 17 (2016) 181-190.